ARMY RESEARCH LABORATORY

Survey of Thermoelectric and Solar Technologies as Alternative Energy Solutions

by Kendall Bianchi, Jay R. Maddux, Kimberly Sablon-Ramsey, and Patrick J. Taylor

NOTICES

Disclaimers

The findings in this report are not to be construed as an official Department of the Army position unless so designated by other authorized documents.

Citation of manufacturer's or trade names does not constitute an official endorsement or approval of the use thereof.

Destroy this report when it is no longer needed. Do not return it to the originator.

Army Research Laboratory

Adelphi, MD 20783-1197

ARL-TR-5920   **February 2012**

Survey of Thermoelectric and Solar Technologies as Alternative Energy Solutions

Kendall Bianchi
Wellesley College
106 Central St., Wellesley, MA, 02481

Jay R. Maddux, Kimberly Sablon-Ramsey, and Patrick J. Taylor
Sensors and Electron Devices Directorate, ARL

REPORT DOCUMENTATION PAGE

1. REPORT DATE *(DD-MM-YYYY)*	2. REPORT TYPE	3. DATES COVERED (From - To)
February 2012	Final	

4. TITLE AND SUBTITLE	5a. CONTRACT NUMBER
Survey of Thermoelectric and Solar Technologies as Alternative Energy Solutions	
	5b. GRANT NUMBER
	5c. PROGRAM ELEMENT NUMBER

6. AUTHOR(S)	5d. PROJECT NUMBER
Kendall Bianchi, Jay R. Maddux, Kimberly Sablon-Ramsey, and Patrick J. Taylor	
	5e. TASK NUMBER
	5f. WORK UNIT NUMBER

7. PERFORMING ORGANIZATION NAME(S) AND ADDRESS(ES)	8. PERFORMING ORGANIZATION REPORT NUMBER
U.S. Army Research Laboratory ATTN: RDRL-SEE-I 2800 Powder Mill Road Adelphi, MD 20783-1197	ARL-TR-5920

9. SPONSORING/MONITORING AGENCY NAME(S) AND ADDRESS(ES)	10. SPONSOR/MONITOR'S ACRONYM(S)
	11. SPONSOR/MONITOR'S REPORT NUMBER(S)

12. DISTRIBUTION/AVAILABILITY STATEMENT

Approved for public release; distribution unlimited.

13. SUPPLEMENTARY NOTES

14. ABSTRACT

Thermoelectric and solar power generation are two promising alternative energy solutions for the military. Power generation devices based on these two technologies aid the military by lightening Soldiers' loads and allowing them to carry fewer batteries and more equipment. Since these technologies use renewable energy sources, Soldiers are also spared the nuisance of having to constantly resupply. Thermoelectric power generates electricity from any adventitious source of heat, while solar cells employ sunlight to do the same. Both technologies are currently subject to extensive research to improve efficiency, utility, and cost. Although they both operate on renewable energy sources, each technology functions at a different temperature range. Thermoelectric devices run on low temperatures, generally below 1000 K, while solar cells require temperatures equivalent to those of the sun. Thermoelectric and solar power generators complement each other since they are capable of producing electricity from disparate sources. Solar produces highly efficient power during daytime but fails in darkness. Thermoelectrics can produce electricity with lower efficiency but dramatically more sources of heat are available for thermoelectric power generation, enabling full diurnal operation. This report discusses measurements of the properties and efficiency of a thermoelectric device and a solar cell.

15. SUBJECT TERMS

Thermoelectric power generation, solar power generation, alternative energy

16. SECURITY CLASSIFICATION OF:			17. LIMITATION OF ABSTRACT	18. NUMBER OF PAGES	19a. NAME OF RESPONSIBLE PERSON
a. REPORT	**b. ABSTRACT**	**c. THIS PAGE**	UU	22	Patrick J. Taylor
Unclassified	Unclassified	Unclassified			**19b. TELEPHONE NUMBER** *(Include area code)* (301) 394-1475

Contents

List of Figures

List of Tables

Acknowledgments

INTENTIONALLY LEFT BLANK.

1. Introduction

Thermoelectric and solar technologies are two promising alternative power generation solutions for the military. Power generation devices based on these two technologies aid the military by lightening Soldiers' loads and allowing them to carry fewer batteries and more equipment. Since these solutions use renewable energy sources, Soldiers are also spared the nuisance of having to constantly resupply. Further, given that the planet's energy needs will at least double within the next 50 years, the stage is set for a major energy shortage unless renewable energy can cover the large deficit that fossil fuels can no longer furnish. Public concern has heightened recently as a result of the disastrous environmental pollution from oil spills and the frightening climate consequences of global warming from the combustion of fossil fuels.

Thermoelectric power generates electricity from any adventitious source of heat, while solar cells employ sunlight to do the same. Both technologies are currently subject to extensive research to improve efficiency, utility, and cost. Although they both operate on renewable power supplies, each technology functions at a different temperature range. Thermoelectric devices run on low temperatures, generally below 1000 K, while solar cells require temperatures equivalent to those produced by the sun. Thermoelectric and solar power generators complement each other since they are capable of producing electricity from disparate sources. Solar produces highly efficient power during daytime but fails in darkness. Thermoelectrics can produce electricity with lower efficiency but dramatically more sources of heat are available for thermoelectric power generation, enabling full diurnal operation

Thermoelectric power generation can provide both energy production and cooling. Thermoelectric power generators are increasingly being used to produce energy out of waste heat—for example, the U.S. Department of Energy manages programs to augment the electrical power needs on board cars by converting the heat emitted by exhaust pipes on cars directly to electricity. Further, thermoelectric cooling is frequently used for handheld coolers and refrigerators. The technology also serves a variety of other purposes, such as measuring temperature in thermometers or powering electronic devices, such as watches. Despite its relatively low efficiency and moderate cost, its benefits include compactness, simplicity, covertness, and reliability.

Solar power is an abundant source of clean and renewable energy. The supply of energy from the Sun to the Earth is gigantic—$3 \cdot 10^{24}$ joules per year, or about 10,000 times more than mankind's current consumption. Nevertheless, the United States solar energy usage is still <1%, primarily due to the high cost associated with fabricating solar cell devices. One approach to driving the cost down is by developing novel techniques for enhancing the efficiency of solar cells. This will reduce the amount of solar cells required to generate power, thereby reducing the overall module costs. For this reason, the U.S. Army Research Laboratory (ARL) has focused

efforts on enhancing the efficiency of solar cell devices in order to reduce the "floatation" cost associated with providing hundreds of batteries to Soldiers in remote locations, and consequently, extend the duration of missions critical in providing real-time intelligence and surveillance to warfighters. Solar cells are an attractive solution because they require little maintenance, have no moving parts, operate on a renewable and cost-free light source, and have a long life span.

This report discusses measurements of the properties and efficiency of a thermoelectric device and a solar cell.

2.   Thermoelectric Devices

The ability of a thermoelectric power generation device to produce electricity is governed by the properties of the materials from which it is constructed. There are three principal thermoelectric properties of a material: the Seebeck coefficient, α; the electrical resistivity, ρ; and the thermal conductivity, κ. Efficient thermoelectric materials have large Seebeck coefficient values, low thermal conductivity values, and small electrical resistivity values. A thermoelectric device generates electricity from a temperature difference, ΔT, by producing a voltage, which generates current. The Seebeck coefficient is the relation between the voltage produced and the applied ΔT; a high value of α generally indicates high efficiency.

In this report, measurement results taken from two different thermoelectric materials, bismuth telluride (Bi_2Te_3) and lead telluride (PbTe), as well as results taken from a fully fabricated thermoelectric power generator, are presented. The Seebeck coefficient, thermal conductivity, resistance, and resistivity were all measured at room temperature. Electrical power, however, is proportional to $(\alpha*\Delta T)^2$, so we chose to measure the power and efficiency of PbTe, which can be heated to a larger ΔT compared with Bi_2Te_3. We used values obtained through the same procedures we used in the first experiments, as well as other known factors involved in the experiment, to calculate the power generated and efficiency as a function of ΔT of the PbTe device.

2.1   Seebeck Coefficient

The first property measured was the Seebeck coefficient. To do this, we placed a sample of Bi_2Te_3 in between two copper plates, which have known values of α. We used a power supply to apply heat to one side of the copper, inducing a ΔT. We used thermocouples attached to both sides to measure ΔT and copper wire probes connected to a voltmeter to measure the voltage, V, across the sample of Bi_2Te_3. Then, a voltmeter measured the voltage across the material for selected values of ΔT. Figure 1 shows a graph of the data points we obtained. The graph of $V(\Delta T)$ showed the slope, equivalent to α of Bi_2Te_3, to be 229 $\mu V/K$.
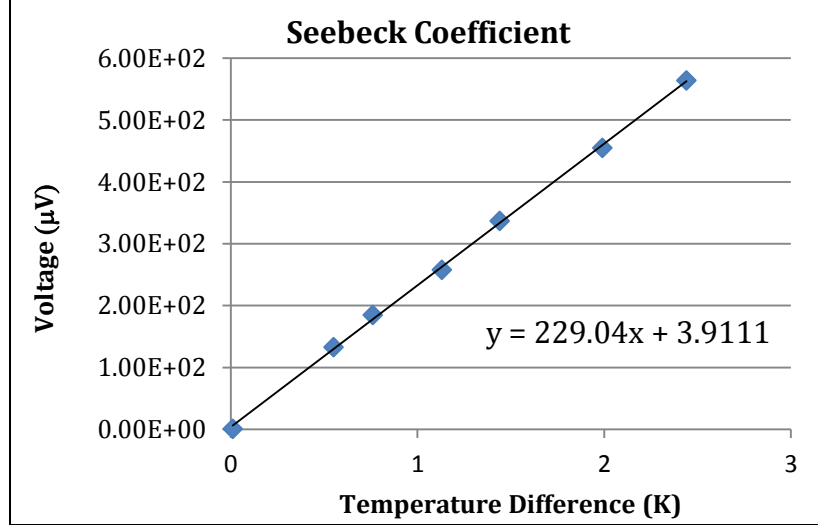
2

Figure 1. Voltage data as a function of temperature difference for Bi_2Te_3.

Note that there is a non-zero intercept of 3.9111 µV. This is believed to derive from an unintended offset voltage somewhere in the experiment. However, this offset voltage source of error is eliminated as a source of error in this work because we are taking the slope, or derivative, of the data. So, in this analysis, any observed offset voltage is irrelevant.

2.2   Thermal Conductivity

The second property measured was the thermal conductivity of the material. For this experiment, we measured the current and temperature needed to heat the cold side of the device until the temperature difference across it was equal to zero. These measurements allowed us to calculate the Peltier heat, Q_Π, using the equation for the first Kelvin relationship:

$$Q_\Pi = \alpha*I*T. \tag{1}$$

We then used Fourier's Law for heat conduction,

$$Q = \Delta T*\kappa*(A/\ell), \tag{2}$$

and assumed $Q = Q_\Pi$ to solve for κ of the sample of Bi_2Te_3 at a given ΔT. In Fourier's law, A is the cross-sectional area and ℓ is the length of the material. As shown in figure 2, the Q as a function of ΔT data is presented; the slope of the data was directly proportional to the thermal conductivity of the material and the area-to-length ratio as (slope = $\kappa*(A/\ell)$).
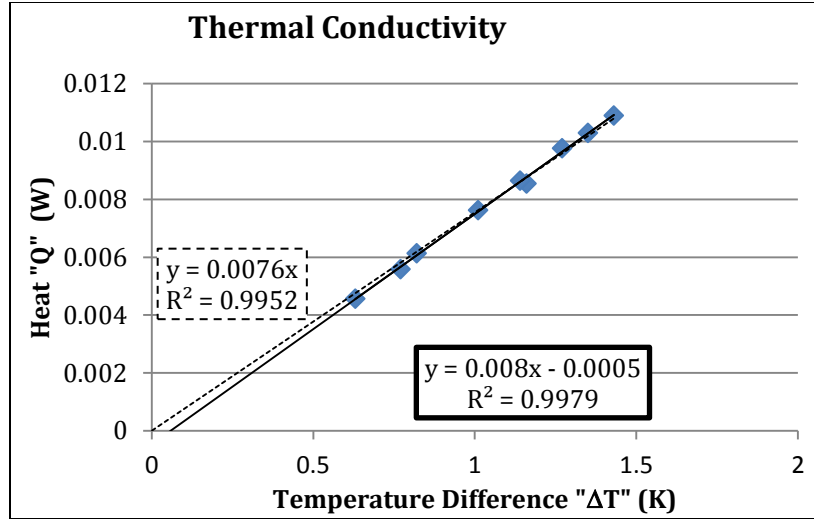
3

Figure 2. Heat flow data as a function of temperature difference for Bi_2Te_3.

In figure 2, we examine two curve-fitting relationships for the observed data; both are shown: the dashed line fit is forced to intercept the origin of the plot and the solid line is allowed to freely maximize the agreement between the data and the linear fit. In either curve-fitting relationship, there is outstanding agreement as reflected by the near unity value of R^2, where R is the correlation coefficient. Assuming the case where the slope is 0.0076 and the $(A/\ell) = 0.51$ cm^2/cm, then we obtain a κ of 14.80 mW/cm-K.

Then, to reduce the error produced by temperatures that were either too high or too low, we graphed thermal conductivity as a function of temperature difference. As shown in figure 3, the y-intercept—or the value of κ when the temperature difference was equivalent to the original value of ΔT—of this overshoot/undershoot graph served as a more accurate reading of the thermal conductivity of the device. However, we noticed that there was a small dependence on the imposed ΔT. To correct for this, as shown in figure 4, we plotted the actual y-intercepts as a function of imposed ΔT and extrapolated to an imposed ΔT of zero. From this extrapolation, we obtained a final thermal conductivity value of 14.21 mW/cm-K.
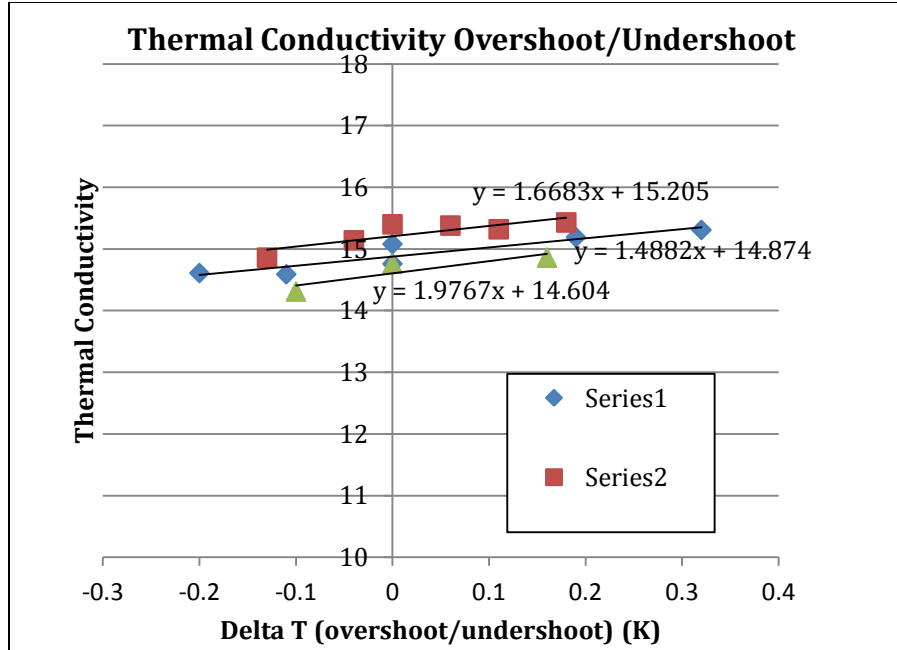
Figure 3. Overshoot-undershoot plot to determine thermal conductivity for Bi_2Te_3.
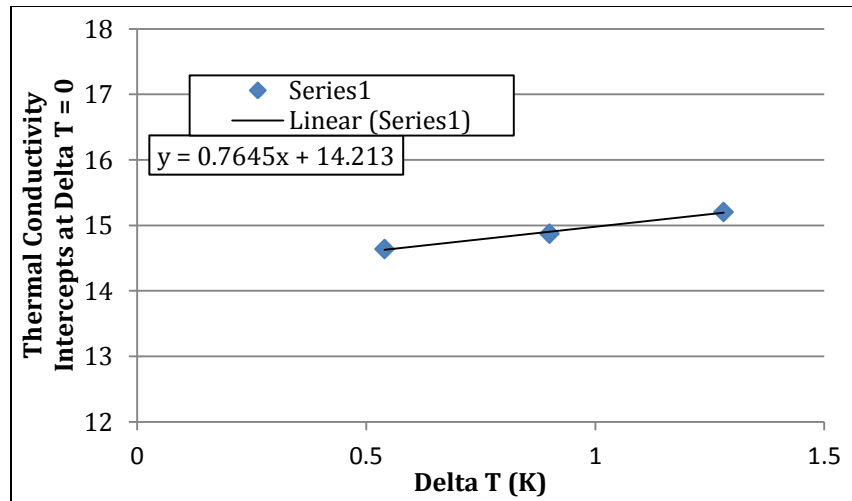

Figure 4. Extrapolated thermal conductivity at $\Delta T=0$ for Bi_2Te_3.

2.3   Resistance and Resistivity

The last two properties we determined were the resistance, R, and resistivity, ρ. To perform this experiment, we used a voltmeter to measure the voltage produced by an applied current, I. Ohm's Law describes the relationship between V, I, and R as

$$V=I*R. \tag{3}$$

The slope of the graph of V(I) revealed the resistance of the device to be approximately 2.8 mΩ. Since $\rho = R(A/\ell)$, the resistivity could then be calculated by multiplying the resistance by A and dividing by ℓ. As shown in final form in figure 5, the slope shows that the calculated resistivity was 1.4 mΩ-cm.
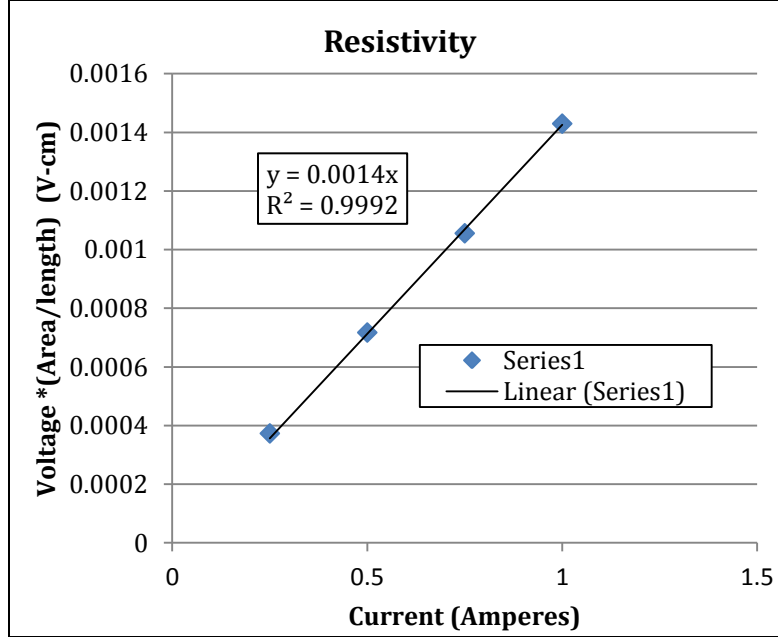

Figure 5. Ohm's law determination of the electrical resistivity for Bi$_2$Te$_3$.

2.4   Power and Efficiency

Because PbTe is more refractory than Bi$_2$Te$_3$, we constructed a complete PbTe device so that the output power, P$_{output}$, and conversion efficiency could be determined at high temperature. The device is shown in figure 6. In order to perform the calculations of power and efficiency for this PbTe device, we used measurements that were, for the most part, obtained through the same procedures as the ones we used to measure the properties of the standalone sample of Bi$_2$Te$_3$. To apply heat energy into the thermoelectric device, we placed a commercial high-temperature heater on top of the device. To measure the temperature difference and P$_{output}$, we positioned thermocouples on both the hot side and the cold side of the device, and connected the output terminals of the device to a voltmeter.

Figure 6. PbTe thermoelectric
power generator device.

To prevent the device from oxidizing and burning, we positioned the whole setup inside a
vacuum bell jar and evacuated that to a base vacuum pressure of 10^{-3} Torr. The power supply
used to warm the heater was set at several gradually increasing power levels, and that yielded
sequentially increasing ΔT values across the thermoelectric device. Because of experimental
limitations, the power supply that warmed the heater was limited to just 60% of the maximum
power. Even with that limitation, sufficient data were collected to perform a complete analysis.
The experiment began by recording the initial conditions before any heater power was supplied
(0%). Successively larger heater powers were then applied to the heater, and the ΔT across the
thermoelectric device rose dramatically. When the ΔT across the device was stable and invariant
with time, the P_{output} that corresponded to the specific ΔT was recorded. For this experiment, the
definition of P_{output} is the maximum power delivered to an impedance-matched load, and the
equation for P_{output} is open circuit voltage squared $(\Delta V_{oc})^2$ divided by four times the internal
device resistance (R_{int}). Figure 7 shows quadratic output power as a function of imposed
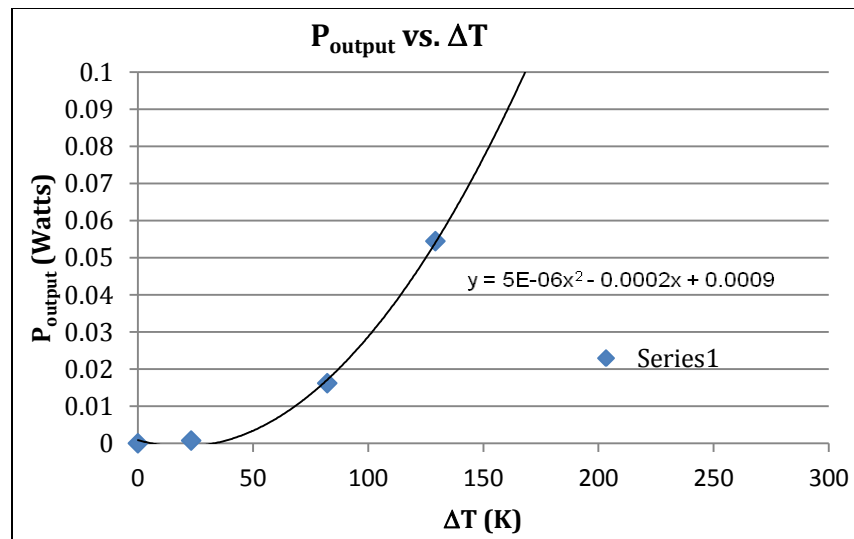temperature difference, ΔT.

Figure 7. Quadratic output power as a function of imposed temperature difference, ΔT.

7

Using these data, which had relatively low ΔT values, we were able to analyze the performance and estimate the P_{output} and efficiency of the device at higher ΔT values.

The P_{output} and efficiency as a function of temperature difference were fit with the equations:

$$\text{Efficiency} = 0.0003(\Delta T)^2 + 0.0122(\Delta T) + 0.0186 \tag{4}$$

$$P_{output} = 5E{-}06(\Delta T)^2 - 0.0002(\Delta T) + 0.0009 \tag{5}$$

Our results anticipated good efficiency values for the temperature differences and power supply levels that were tested. As presented in figure 8, with the 60% maximum power to the heater, we observed an efficiency of 5.96%, and had we obtained ΔT and voltage data points with the power supply up to 80%, our graphs suggest we would have observed an efficiency of between 9 and 10%.
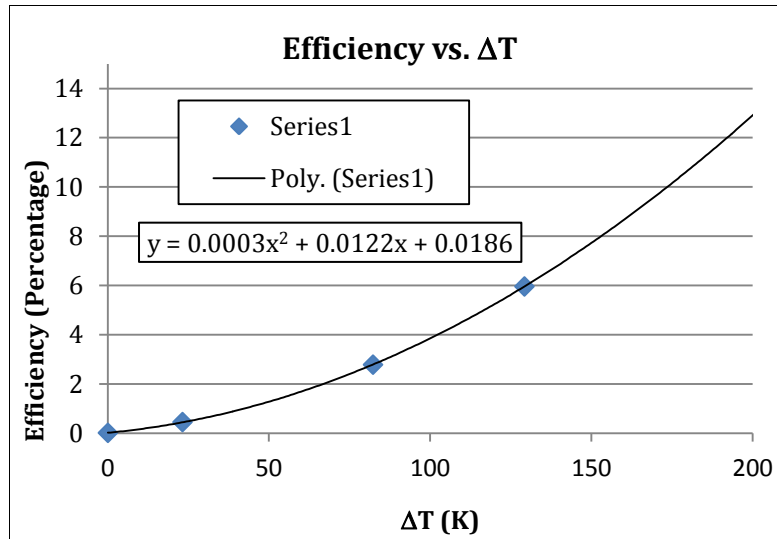

Efficiency vs. ΔT

$y = 0.0003x^2 + 0.0122x + 0.0186$

Figure 8. Quadratic output power as a function of imposed temperature difference, ΔT.

3. Quantum-dot Solar Cells

Solar cells consist of a p-n junction that is created when one side of the semiconductor material is doped to provide a high concentration of acceptor atoms (p-side) and the other side is doped to provide a high concentration of electrons (n-side). When photons from sunlight hit a solar module, they are absorbed by the solar cells. Inside the semiconductor material, electrons within the atoms absorb the energy and are knocked loose from the valence band to the conduction band, a higher energy level. The minimum energy required for the electrons to make this transition is called the bandgap (E_g). Photons that hit the solar cell must have a minimum energy (E_{ph}) to excite the electrons enough to move them from the valence band up to the conduction band. If $E_{ph} \geq E_g$, the electrons will have enough energy to cross the bandgap. This extra energy

allows the electrons to flow across the p-n junction and through a circuit, producing current and voltage. The movement of an electron from the valence band to the conduction band leaves behind a "hole," which effectively creates a positive charge through the absence of the electron. Holes "move" when other electrons fill the gap, and thus can also participate in conduction.

However, in a non-ideal solar cell device, photons have energies that are either greater or less than the bandgap of the semiconductor material (if $E_{ph} < E_g$ or $E_{ph} > E_g$). In the case of $E_{ph} > E_g$, photon energy is lost as heat, and in the case of $E_{ph} < E_g$, photons cannot be absorbed. These two cases have limited the efficiency of solar cells to 31%. Therefore, to exceed this efficiency limit concepts, we need to either enable the absorption of photons above-bandgap or below-bandgap. Therefore, this project concentrated on the absorption of below-bandgap photons by using quantum dots (QDs) for enhancing the efficiency of solar cells. QDs are very promising candidates with the potential to create energy levels that can better match the solar spectrum provide greater freedom in absorption band and strain engineering as compared to their bulk counterparts with predicted efficiencies of ~64%. However, experimental results are substantially lower than this limit. This is because introducing QDs into the solar cells gives rise to additional channels of recombination, which increase the recombination losses. To minimize the recombination losses in QD solar cells, we identified the physical mechanisms that control recombination processes in QDs heterostructures and proposed a novel approach for improving the basic parameters of QD solar cells, which is based on a quantum dot with a built-in charge (Q-BIC) structure.

However, this aspect of the project investigates the solar cell parameters prior to integrating the Q-BIC technology. To investigate the effects of incorporating QDs into the intrinsic region of a single junction gallium arsenide (GaAs) solar cell as well as the effect of manipulating the wetting layer states, different device configurations were explored. We compared the GaAs reference cell to a standard QD cell (InAs/GaAs) and a QD cell containing a thin aluminium gallium arsenide (AlGaAs) layer (InAs/AlGaAs/GaAs) for both p-i-n and n-i-p configurations. The AlGaAs layer was introduced as a way of manipulating the wetting layer states. While multi-stacks of QDs are required for enhancing the absorption of low-energy photons, carriers may become trapped by the wetting layer of subsequent stacks and recombine before they are collected.

To determine the solar cell efficiency η, various parameters such as the short-circuit current (I_{SC}), open-circuit voltage (V_{OC}), and the fill factor (FF) should be evaluated. These parameters can be determined from the current-voltage (I-V) characteristics of the device (figure 9).
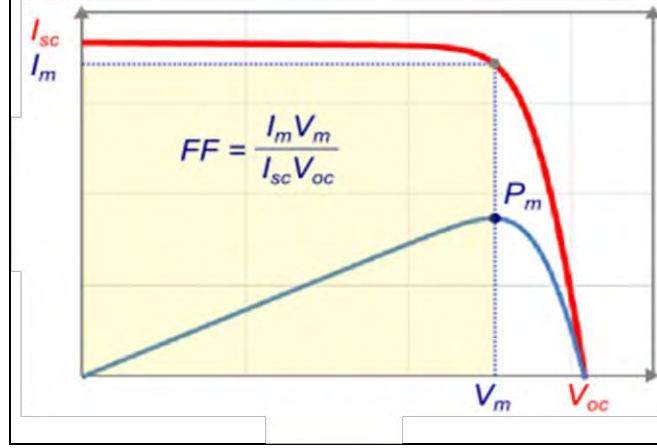
Figure 9. Illustration of I-V characteristics under illumination.

When light hits the solar cell sample, it shifts the I-V curve such that maximum values for current and voltage—short-circuit current and open-circuit voltage—can be obtained; I_{SC} is the current at $V = 0$ and V_{OC} is the voltage at $I = 0$. The fill factor measures the "squareness" of the I-V curve, or the ratio of the maximum power value (as a function of voltage) to the product of I_{SC} and V_{OC}. The efficiency is defined as the ratio of the power output to the power input and is measured using values for I_{SC}, V_{OC}, and the fill factor. The maximum current (I_M) and voltage (V_M) generated by the device is crucial for calculating the fill factor (equation 6) and efficiency (equation 7):

$$FF = \frac{I_m V_m}{I_{sc} V_{oc}} \tag{6}$$

$$\eta = \frac{FF I_{sc} V_{oc}}{P_{in}} \tag{7}$$

The efficiency of the photovoltaic conversion in our n-i-p and p-i-n solar cell devices with and without AlGaAs was measured using a calibrated solar simulator. The corresponding I-V curves for p-i-n and n-i-p devices under 1 Sun (AM1.5 G) irradiation are presented in figure 10. For comparison, in figure 10, we also presented I-V curves for the reference cell without QDs. As seen, the short-circuit current decreases from ~14.7 mA/cm^2 in the p-i-n reference cell to ~13.2 mA/cm^2 and similarly, the V_{OC} decreased from 0.8 to 0.6 V, respectively. The QD samples with and without AlGaAs layers in the n-i-p configuration also showed deterioration in the device performance (table 1). This can be attributed to the processing conditions for devices grown on a p-GaAs buffer layer using semi-insulating substrates.
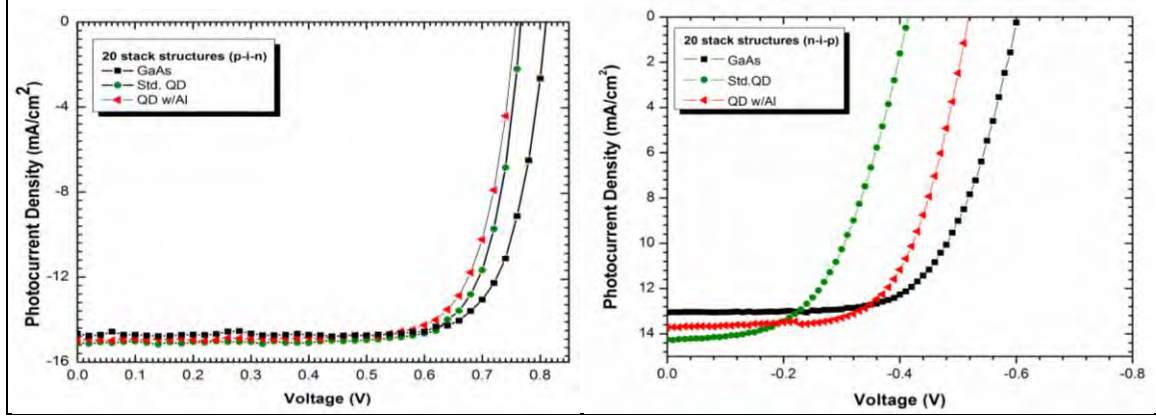
10

Figure 10. I-V characteristics of solar cells with and without an AlGaAs layer (left) a p-i-n configuration and (right) n-i-p configuration.

Table 1. Calculated solar cell parameters of the devices explored: GaAs reference, and QD with and without AlGaAs layers.

Structures	P-i-N Structures				N-i-P Structures			
	J_{SC} (mA/cm^2)	V_{OC}(V)	FF (%)	η (%)	J_{SC} (mA/cm^2)	V_{OC}(V)	FF (%)	η (%)
GaAs Ref.	14.66	0.81	79	9.8	13.2	0.62	39	2.3
Std. QD	15.07	0.77	77	9.3	14.4	0.41	18	1.08
QD with AlGaAs	14.97	0.71	77	8.9	13.6	0.53	18	1.82

In order to determine the harvesting role of infrared (IR) photons in the QD devices, we measured the spectral dependence of the photocurrent under low illumination conditions using a Nicolet Fourier transform infrared (FTIR) spectrometer. Figure 11 shows the photoresponse of the GaAs reference cell and QD devices with and without an AlGaAs layer.
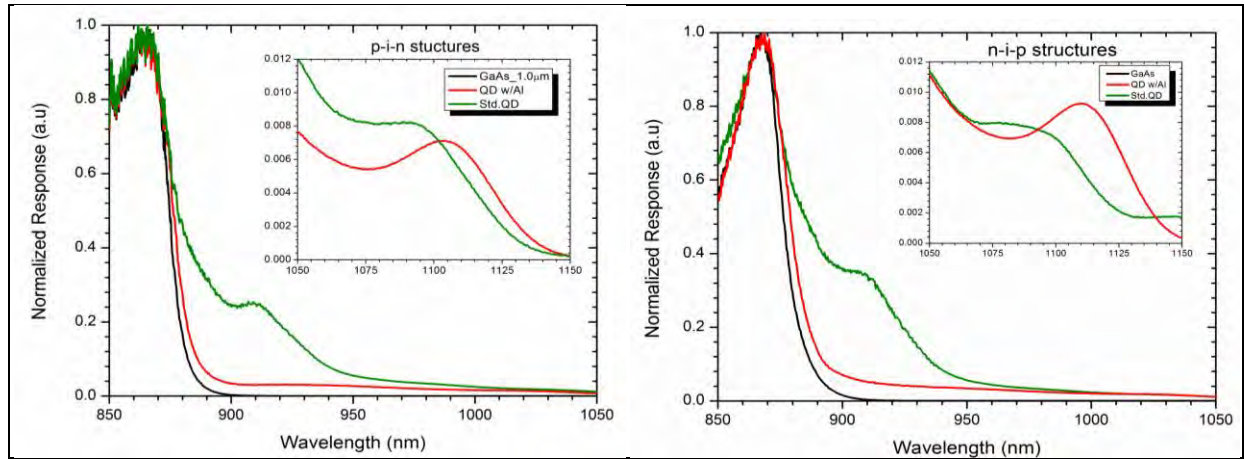

Figure 11. Spectral response of the GaAs reference, QD structures with and without AlGaAs layers. The insets show magnified views of the spectral response contribution from the QD structures. (left) p-i-n device configuration and (right) n-i-p device configuration.

11

From figure 11, we observe the band-to-band absorption in the GaAs matrix below ~880 nm. Transitions in the range from 880 to 920 nm correspond to the wetting layer. Transitions above 920 nm are most likely related to the various excited QD states. Finally, the ground state transition in QDs is ~1100 nm as shown in the insets on both sides of the figure 11. As seen, the photoresponse due to the wetting layer states is completely reduced in the samples containing the AlGaAs layers and the long wavelength contribution enhances substantially in the n-i-p structures compared with the p-i-n devices.

4. Conclusion

In summary, we measured the properties and efficiency of a thermoelectric device and a solar cell. For thermoelectric devices, we measured the three principal thermoelectric properties of Bi_2Te_3 at room temperature. We determined a Seebeck coefficient of 229 μV/K, an electrical resistivity of 1.4 milliOhm-cm, and a thermal conductivity of 14.21 mW/cm-K. To determine the efficiency and output power at higher temperature, a PbTe-based thermoelectric device was constructed and tested. Although the temperature difference was limited to somewhat low values, we measured 54 mW at a temperature difference of 129 K. The device successfully converted heat energy to electricity with 6% conversion efficiency at a temperature difference of 129 K. Because the output power is proportional to ΔT^2, curves of this family can be fitted to the obtained data, and doing so, we estimate that the device would produce nearly 150 mW at a temperature difference of 250 K, with an efficiency near 12%. These experiments confirmed PbTe's effectiveness as one of the more popular thermoelectric materials. Both Bi_2Te_3 and PbTe exhibited excellent thermoelectric properties, and both displayed great potential in the field of alternative energy solutions.

For the solar cell, our investigation showed that while QD technology is far from ideal, it shows promise in its capabilities to extend the spectral range that can be absorbed in conventional GaAs solar cells. To accurately evaluate the effects of the AlGaAs layers on the carrier transport properties, the n-i-p structures should be regrown on p-type GaAs substrates rather than beryllium (Be)-doped GaAs to minimize the non-radiative recombination processes due to Be cluster-type defects.

List of Symbols, Abbreviations, and Acronyms

AlGaAs	aluminium gallium arsenide
ARL	U.S. Army Research Laboratory
Be	beryllium
Bi_2Te_3	bismuth telluride
FTIR	Fourier transform infrared
GaAs	gallium arsenide
InGaAs	indium gallium arsenide
IR	infrared
PbTe	lead telluride
Q-BIC	quantum dot with a built-in charge
QDs	quantum dots